Automatic Detection of Welding Defects using Deep Neural Network

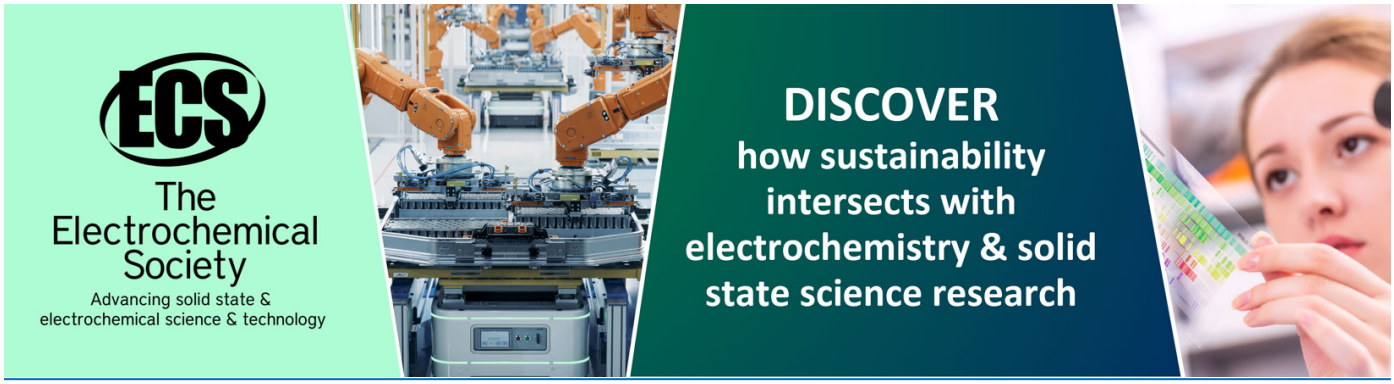

Automatic Detection of Welding Defects using Deep Neural Network

Wenhui Hou, Ye Wei, Jie Guo, Yi Jin, Chang'an Zhu

School of Engineering Science, University of Science and Technology of China, Hefei, People's Republic of China

E-mail: jinyi08@ustc.edu.cn, hwh303@mail.ustc.edu.cn

Abstract. In this paper, we propose an automatic detection schema including three stages for weld defects in x-ray images. Firstly, the preprocessing procedure for the image is implemented to locate the weld region; Then a classification model which is trained and tested by the patches cropped from x-ray images is constructed based on deep neural network. And this model can learn the intrinsic feature of images without extra calculation; Finally, the sliding-window approach is utilized to detect the whole images based on the trained model. In order to evaluate the performance of the model, we carry out several experiments. The results demonstrate that the classification model we proposed is effective in the detection of welded joints quality.

1. Introduction

With the increasing requirement for the quality of equipment, radiographic testing as one of the oldest non-destructive testing (NDT) is commonly used in the detection of welded joints quality in many industrial fields such as the nuclear, chemical and aeronautical [1]. The real-time detection and automatic identification for welding defects from the digitized gray images become the focus of NDT research. In the last three decades, several efforts have been devoted to the development of such a system which can detect and classify the welding defects automatically using X-ray images.

D Mery [2] proposed a scheme for detecting weld defects from digitized film images based on three steps: segmentation, texture features extraction and classification. The supreme precision of the system achieved 90.91%. Silva et al. [3] described a non-linear classifier based on artificial neural networks (ANNs) compared with the linear classifiers. A criterion of neural relevance was applied to evaluate the capacity of the classifier studied by the geometric features in order to prove that the quality of the features extracted is more important than the quantity of the features. And Jayendra Kumar et al. [4] extracted the texture features in different direction for several spatial pixel distances for classifying the different flaws and obtained an overall classification accuracy of 86.1% by using artificial neural network (ANN). In another work [5], they integrated texture and geometrical feature, and obtained an accuracy of 87.34%. While Gang Wang and Liao [6] implemented an automatic computer-aided identification system. Twelve numeric features extracted were sent into two classifiers: fuzzy k-nearest neighbor (fuzzy K-NN) and multi-layer perceptron (MLP) neural networks for classifying different flaw types. Mohamed S. Juan Zapata [7] described an adaptive-network-based fuzzy inference system (ANFIS) for recognizing welding defects in radiographic images. In this work, 12 geometrical features is chosen as the input of ANFIS. Ioannis Valavanis [8] used sequential

backward selection (SBS) method to select useful features for reducing the computational burden, and they compared the accuracies of three different classifiers.

These systems mainly rely on three steps : digital image processing, feature extraction, and pattern recognition. The image processing is designed to locate the weld region and segment the potential defects from the x-ray image. Miguel Carrasco and Domingo Mery [9] directly used digital image processing techniques including noise attenuation filters, edge detection techniques, the watershed transform, and the distance transform to segment welding defects without the later steps. Nevertheless, the quantitative evaluation of the system performance is more complex. In the phase of feature extracting, the texture and geometrical features were commonly used. Usually these features are numerous and the calculations are complex. In addition, not all the features are sensitive to classification, thus the feature selection relying on artificial selection, sequential forward selection (SFS), multi-scale wavelet packet (MWP), Hough transform or principal components analysis (PCA) is essential in order to reduce the dimension of the features.

Nowadays, modern computer vision techniques, such as deep learning [10] and sparse coding [11] are providing a new way in detecting the object automatically from optical images. In this paper, an automatic classification model based on deep neural network is proposed. It implements unsupervised learning for intrinsic feature representation by using several sparse auto-encoders (SAEs) instead of calculating the texture or geometrical features and extra feature selection. Then the softmax regression with supervised learning is used to fine-tune the deep network. And the proposed model is trained and tested by the x-ray image patches. In addition, we utilize the trained model to inspect the whole image and find the defects region. And the results demonstrate that the classification model we proposed is enough effective in the detection of welded joints quality.

2. Deep neural network

2.1. sparse auto-encoder

Sparse auto-encoder (SAE) network including input layer, hidden layer and output layer is mainly used for unsupervised learning [12]. The structure is shown in Figure 1.

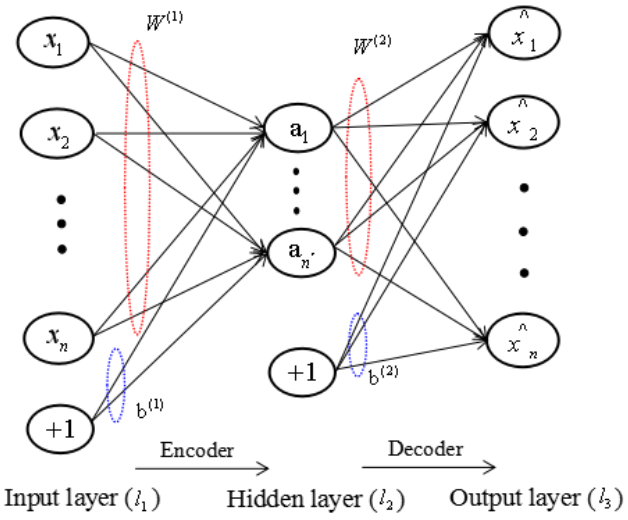

Figure 1. The structure of SAE

As is shown in figure 1, this network includes two parts. The one is encoder which is from input layer to hidden layer, $\mathbf{W}^{(1)}$ and $\mathbf{b}^{(1)}$ are the weight matrix and the bias of this part. The other one called decoder is from hidden layer to output layer, $\mathbf{W}^{(2)}$ and $\mathbf{b}^{(2)}$ are the corresponding parameters of this part.

The network tries to reconstruct the input vector in output layer, as is shown in Eq.1

$$\hat{\mathbf{x}} = h_{W,b}(\mathbf{x}) \approx \mathbf{x} \tag{1}$$

Where $\mathbf{x}$ is the input vector $\mathbf{x} \in R^{n\times 1}$. The cost function of SAE is given by

$$J(\mathbf{W},\mathbf{b}) = \{\frac{1}{m}\sum_{i=1}^{m}[\frac{1}{2}\left\|h_{W,b}(\mathbf{x}^{(i)}) - \mathbf{x}^{(i)}\right\|^2]\} + \frac{\lambda_1}{2}\sum_{l=1}^{2}\sum_{i=1}^{s_l}\sum_{j=1}^{s_{l+1}}(W_{ji}^{(l)})^2 + \beta\sum_{j=1}^{s_2}KL(\rho\left\|\hat{\rho}_j\right.) \tag{2}$$

The first part of the function is the mean square term minimizing the error between the input data and the output data. $\mathbf{x}^{(i)}$ represent the ith sample, m is the amount of the samples. For each sample, $h_{W,b}(\mathbf{x}) = \sigma(\mathbf{W}^{(2)}\mathbf{a} + \mathbf{b}^{(2)})$ is the function of decoder, where $\mathbf{W}^{(2)} \in R^{n\times n'}$, $\mathbf{b}^{(2)} \in R^{n'\times 1}$. And $\mathbf{a}$ is the activation of hidden layer given by: $\mathbf{a} = \sigma(\mathbf{W}^{(1)}\mathbf{x} + \mathbf{b}^{(1)})$, i.e. the function of encoder. Where $\mathbf{W}^{(1)} \in R^{n'\times n}$, $\mathbf{b}^{(1)} \in R^{n'\times 1}$, σ is the sigmoid function, expressed as $(1+\exp(-x))^{-1}$, i.e. the activation function of encoder and decoder.

The second part of the function is the regularization term, also called the weight decay term avoiding over-fitting. Where λ_1 is the regularization factor, s_l represents the number of units in layer l which is equal to 3 in our network, and obviously, $s_1 = n$, $s_2 = n'$, $s_3 = n$. $W_{ji}^{(l)}$ is the weight between the i th unit in layer l and the j th unit in layer l+1.

The last part of the function is the sparse penalty term which impose a sparsity constraint on the hidden units, where β is the weight of this term. Kullback–Leibler divergence is given as Eq.3

$$KL(\rho\left\|\hat{\rho}_j\right.) = \rho\log\frac{\rho}{\hat{\rho}_j} + (1-\rho)\log\frac{1-\rho}{1-\hat{\rho}_j} \tag{3}$$

Where ρ is the sparsity parameter which is usually small, $a_j^{(i)}$ represents the activation of the j th hidden unit for the i th sample. $\hat{\rho}_j$ is the average activation of all the samples given by $\hat{\rho}_j = \frac{1}{m}\sum_{i=1}^{m}[a_j^{(i)}]$. The L-BFGS and back propagation are used to train the network for minimizing the cost function.

2.2. Softmax classifier

Softmax classifier uses a supervised learning algorithm for multi-class classification problem. It works according to the probability belong to each category. The cost function is expressed as:

$$J(\boldsymbol{\theta}) = -\frac{1}{m}[\sum_{i=1}^{m}y^{(i)}\log h_{\boldsymbol{\theta}}(\mathbf{x}^{(i)}) + (1-y^{(i)})\log(1-h_{\boldsymbol{\theta}}(\mathbf{x}^{(i)}))] \tag{4}$$

Where $\boldsymbol{\theta} = [\boldsymbol{\theta}_1^T, \boldsymbol{\theta}_2^T, ...\boldsymbol{\theta}_k^T]^T \in R^{k\times(d+1)}$ is the parameters of this modal which is trained by minimizing the function. $\boldsymbol{\theta}_1, \boldsymbol{\theta}_2, ...\boldsymbol{\theta}_k \in R^{d+1}$, $\boldsymbol{\theta}_j^T$ is the jth row of matrix $\boldsymbol{\theta}$. $\mathbf{x}^{(i)} \in R^{d+1}$, k is the number of categories, $h_{\boldsymbol{\theta}}(x)$ represent the probability function belong to each category given by

$$h_{\theta}(x^{(i)}) = \begin{bmatrix} p(y^{(i)}=1|\mathbf{x}^{(i)};\boldsymbol{\theta}) \\ p(y^{(i)}=2|\mathbf{x}^{(i)};\boldsymbol{\theta}) \\ \cdots \\ p(y^{(i)}=k|\mathbf{x}^{(i)};\boldsymbol{\theta}) \end{bmatrix} = \frac{1}{\sum_{j=1}^{k} e^{\boldsymbol{\theta}_j^T x^{(i)}}} \begin{bmatrix} e^{\boldsymbol{\theta}_1^T \mathbf{x}^{(i)}} \\ e^{\boldsymbol{\theta}_2^T \mathbf{x}^{(i)}} \\ \cdots \\ e^{\boldsymbol{\theta}_k^T \mathbf{x}^{(i)}} \end{bmatrix} \tag{5}$$

Where $y^{(i)} \in \{1,2,..k\}$, is the label of the input $\mathbf{x}$. $1/\sum_{j=1}^{k} e^{\theta_j^T x^{(i)}}$ is set to normalize the distribution. The cost function becomes Eq. 6 when a weight decay term is added.

$$J(\boldsymbol{\theta}) = -\frac{1}{m}\left[\sum_{i=1}^{m}\sum_{j=1}^{k} 1\{y^{(i)}=j\}\log\frac{e^{\theta_j^T \mathbf{x}^{(i)}}}{\sum_{l=1}^{k} e^{\theta_l^T \mathbf{x}^{(i)}}}\right] + \frac{\lambda_2}{2}\sum_{i=1}^{k}\sum_{j=1}^{d+1}\theta_{ij}^2 \tag{6}$$

where $1\{\cdot\}$ is the indicator function. λ_2 is the weight decay parameter, θ_{ij} present the weight between the j th unit of input layer and the i th unit of output layer. For each input vector, its category is judged by this classifier as the one whose probability is the maximum value of all categories.

2.3. Deep neural network model

In this part, a classification model based on deep neural network called SSAE was constructed by stacking several SAEs and a softmax classifier.

Firstly, we train SAEs one by one using the unlabeled samples for unsupervised learning. The hidden layer activities of the former SAE are used as the input to train the next SAE. And once the training of each SAE is finished, the decode layers of all SAEs are removed. The outputs of the last SAE are no other than the learned features. Then the Softmax classifier is connected to the rear of SAEs in order to finish the classification task. Lastly, the fine-tuning of the whole network using the labeled samples is a key step for better classification accuracy.

3. Experiment

3.1. The x-ray image set

The x-ray images used in this paper are obtained from a public database called GDXray [13]. The group ‘welds’of the GDXray database is used in this paper. The group contains 88 images arranged in 3 series. The collection of these x-ray images is taken by BAM Federal Institute for Materials Research and Testing, Berlin, Germany. The samples of the proposed model for later learning are mainly selected from series W0001.

3.2. Pre-processing of the images

In this section, the weld region must be isolated from the rest of the elements in the x-ray images. In this way, the burden of identification is reduced. The process is developed in two steps. First, the gray scale image should be converted into a binary image according to an optimal threshold in order to separate an object’s pixels from the background pixels. For this, the Otsu’s method [14] is used which select the optimal threshold by minimizing the intraclass variance of the thresholded black and white pixels. Next, we crop an appropriate rectangular region from the original image according to the binary image for later sample acquisition.

An example of processed results is shown in figure 2.

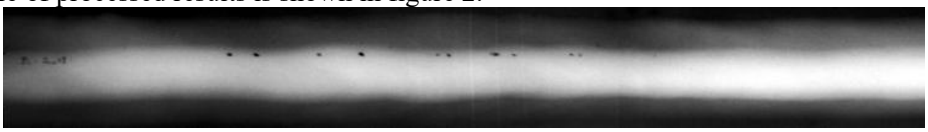

(a) original image

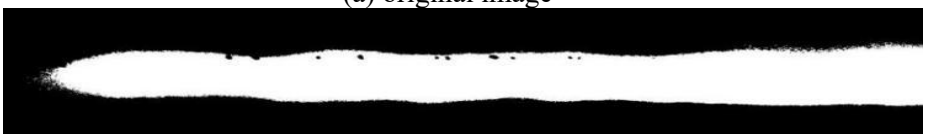

(b) binary image

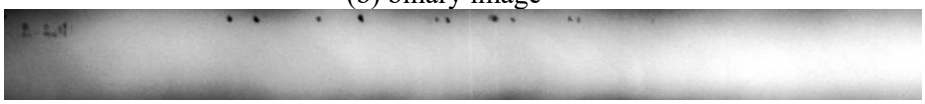

(c) weld region

Figure 2. The result of the processing

3.3. Classification and the detection via the proposed model

We crop patches with the size 32×32 pixels from the processed images as the deep learning sample set. These patches are labeled as 0 (no-defect) or 1 (defect) according to the annotations of bounding boxes. Several examples are shown in figure 3.

Several experiments are implemented including extracting the feature using SAE and examining the classification accuracy under different parameters of the model. In addition, we inspect the whole x-ray image using the slide-window method and recognized the defects through the proposed classification model. Figure 4 shows the overall flowchart of the experimental model.

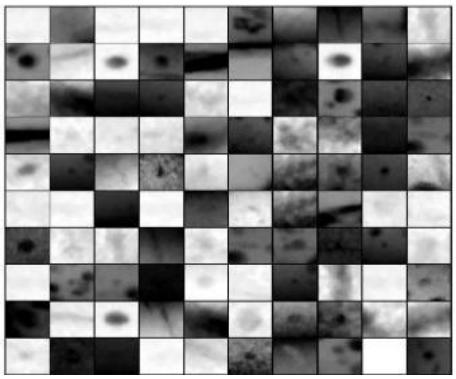

(a) patches with defects

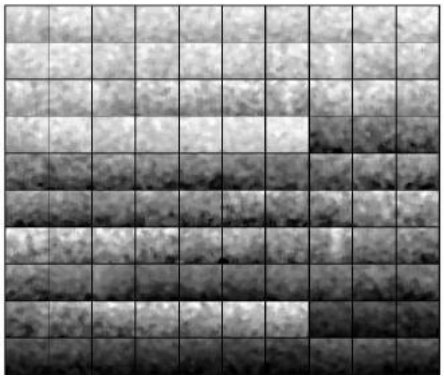

(b) patches with no-defects

Figure 3. The examples of patches

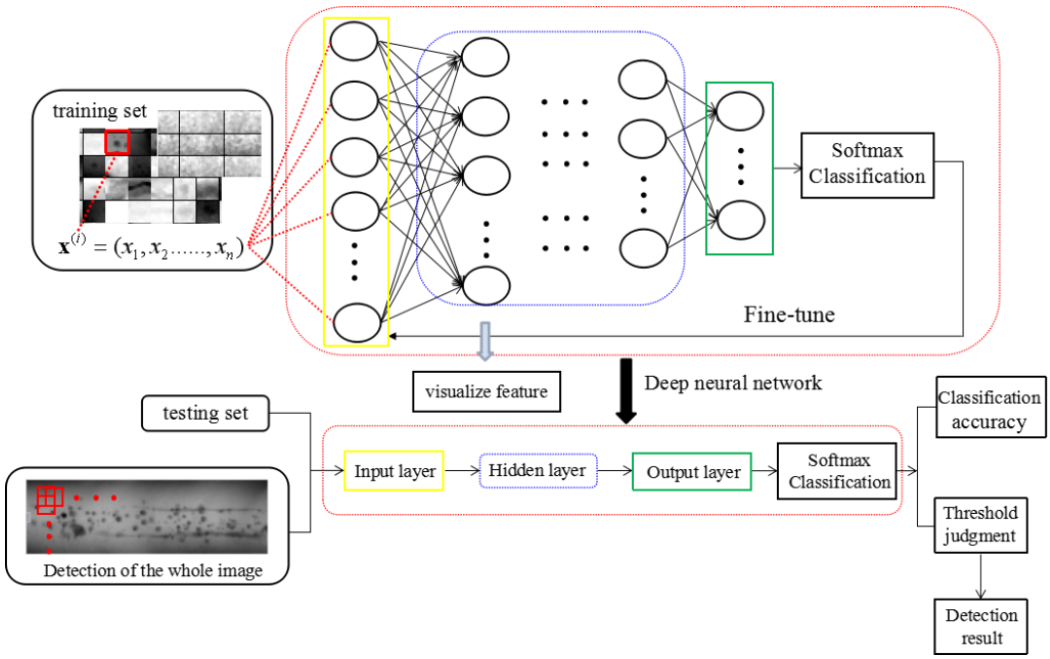

Figure 4. The overall flowchart of the proposed model

4. Experimental results

The performance of the proposed model is discussed through above-mentioned experiments. Next, the results of these experiments are shown in this section.

4.1. The result of unsupervised learning

In order to visualize the bases of image from single SAE, we choose 400 patches randomly from the sample set as the input of SAE. The features learned presenting different orientations and locations are shown in figure 5.

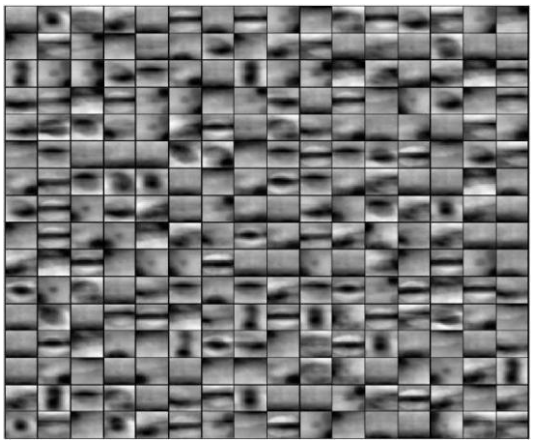

Figure 5. The features learned from SAE

4.2. Deep neural network parameter decision

In this section, in order to find the better parameters of deep neural network for classifying, we carry out several experiments to determine the number of hidden layers, the amount of neurons and the value of the sparsity parameter.

The influence of the number of network layers on classification performance is first examined. Two models with two hidden layers of 576 and 196 neurons and three hidden layers of 576, 196, 100 neurons are implemented, named as DL_net1 and DL_net2 respectively. In order to evaluate the

classification performance of these two networks, we use 5-fold cross validation. So the training and testing are implemented 5 times. Table1 show the results of these 5 times testing for two models.

Table1. The results of testing

model	fold	P_r (%)	R_e (%)	$F1$ (%)	η (%)
DL_net1	1	84.82	90.00	87.33	87.63
	2	89.77	87.78	88.76	89.47
	3	90.34	88.33	89.33	90.00
	4	91.67	85.56	88.51	89.47
	5	83.77	88.89	86.25	86.58
	average	88.07	88.11	88.03	88.63
DL_net2	1	90.27	92.78	91.51	91.84
	2	87.50	89.44	88.46	88.95
	3	94.61	87.78	91.07	91.84
	4	89.77	87.78	88.76	89.47
	5	82.91	91.67	87.07	87.11
	average	89.01	89.89	89.37	89.84

In the table, the precision is presented as $P_r = \frac{TP}{TP+FP}$, the recall is defined as $R_e = \frac{TP}{TP+FN}$, the accuracy is defined as $\eta = \frac{TP+TN}{P+N}$, the F1 score is defined as $F1 = \frac{2 \times P_r \times R_e}{P_r + R_e}$. where TP is the number of defect patches correctly classified, TN is the number of no-defect patches correctly classified, FP is the number of no-defect patches classified as defect patches, FN is the number of defect patches classified as no-defect patches. We observe that accuracy of DL_net2 is about one percentage point higher than that of DL_net1.

The decision of the number of hidden neurons is another problem for the classification model. For this, we investigate the classification performance of two different networks which are DL_net21 with 576 - 196 -100 neurons and DL_net22 with 576 -196-50 neurons. The accuracies of two networks using hold-out testing versus the sparsity parameter changing from 0.04 to 0.12 are plotted in figure 6. The accuracy of DL_net21 achieve the maximum value of 90.9% at $\rho = 0.1$, while the one of DL_net22 achieve the maximum value of 90% at $\rho = 0.08$. Therefore, DL_net21 is adopted in the network adopted for later research and the value of the sparsity parameter selected is 0.1.

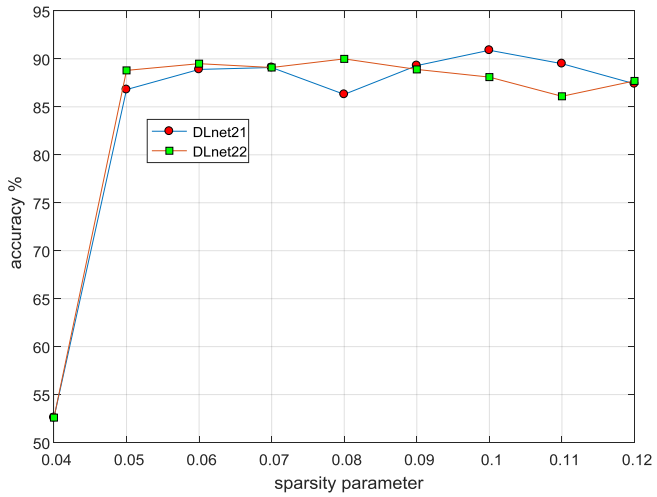

Figure 6. The accuracy versus sparsity parameter

4.3. Identification of defects for whole image

In this section, in order to validate the performance of our classification model, we implement the experiment on the whole x-ray image. For this, the sliding-window approach is adopted. The detection window with the size 32×32 pixels moves on the input image in both horizontal and vertical directions with step of 2 pixels. Every patch under the window is marked as "0" or "1" through the deep neural network. The pixels in the overlap of the detection windows are marked many times, and the mark values are accumulated. For each pixel, the mark value is varied between 1 and 256. When the value is more than an appointed threshold, the pixel is considered as defect. This process is called threshold judgement. The probability map for each pixel judged as a defect is shown in figure 7(a). The original image with the defect region marked is shown in figure 7(b). The results of other images are shown in figure 8.

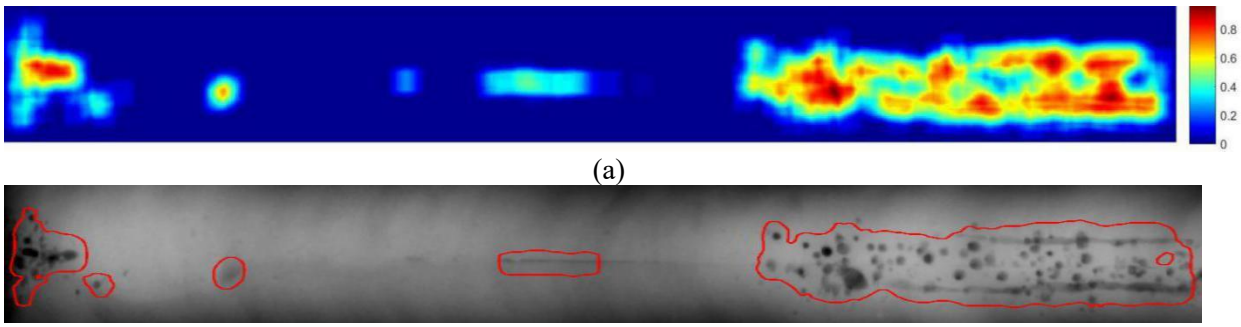

(a)

(b)

Figure 7. (a) The probability map for defects (b) The detection result

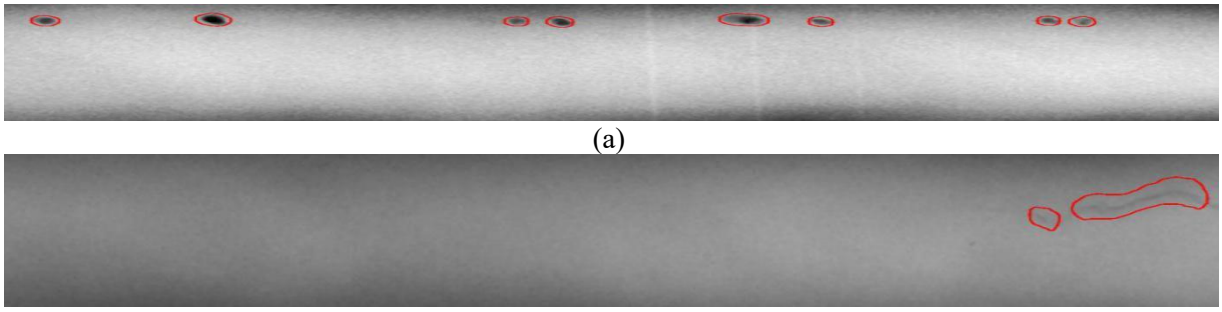

(a)

(b)

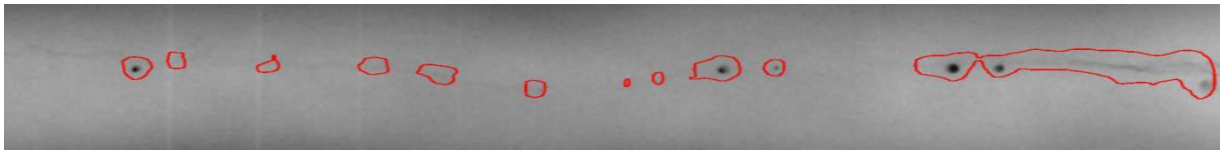

(c)

Figure 8. The detection results of other images

The results show that the proposed model can effectively recognize the defects of different types, such as gas hole, porosity, lack of penetration and crack, etc.

5. Conclusions

In this paper, we present an automatic detection model for weld defect based on deep neural network that extracts the intrinsic features of x-ray images. Several experiments have been conducted to validate our method and the influence of different parameters in the model on classification performance is also analyzed. Furthermore, we adopt the sliding-window approach to detect the whole x-ray image. The experiment results illustrate that the proposed model obtain a maximum classification accuracy rate of 91.84% (with 90.27% precision and 92.78% recall). For the whole images, the experiments of defect inspections are implemented based on the proposed model and the defects can be effectively recognized without distinguishing the specific types of the defects. In the future, we will try to classify the different weld defects of x-ray images.

6. References

[1] Vilar R, Zapata J, Ruiz R. C. 2016. An automatic system of classification of weld defects in radiographic images. NDT & E International 42, 5 (2009), 467 – 476.DOI= http://dx.doi.org/10.1016/j.ndteint.2009.02.004.

[2] D. Mery and M.A. Berti. 2003. Automatic detection of welding defects using texture features. Insight - Non-Destructive Testing and Condition Monitoring 45, 10 (2003), 676 – 681. DOI= http://dx.doi.org/10.1784/insi.45.10.676.52952.

[3] Romeu R.Da Silva, Luiz P. Calôba, Marcio H.s. Siqueira, and João M.a. Rebello. 2004. Pattern recognition of weld defects detected by radiographic test. NDT & E International 37, 6 (2004), 461 – 470. DOI: http://dx.doi.org/10.1016/j.ndteint.2003.12.004

[4] Jayendra Kumar, R.s. Anand, and S.p. Srivastava. 2014. Multi - Class welding flaws classification using texture feature for radiographic images. 2014 International Conference on Advances in Electrical Engineering (ICAEE) (2014). DOI= http://dx.doi.org/10.1109/icaee.2014.6838443

[5] Jayendra Kumar, R.S. Anand, and S.P. Srivastava. 2014. Flaws classification using ANN for radiographic weld images. 2014 International Conference on Signal Processing and Integrated Networks (SPIN) (2014). DOI= http://dx.doi.org/10.1109/spin.2014.6776938

[6] Gang Wang and T.warren Liao. 2002. Automatic identification of different types of welding defects in radiographic images. NDT & E International 35, 8 (2002), 519 – 528. DOI= http://dx.doi.org/10.1016/s0963-8695(02)00025-7

[7] Juan Zapata, Rafael Vilar, and Ramón Ruiz. 2010. An adaptive-network-based fuzzy inference system for classification of welding defects. NDT & E International 43, 3 (2010), 191 – 199. DOI= http://dx.doi.org/10.1016/j.ndteint.2009.11.002

[8] Ioannis Valavanis and Dimitrios Kosmopoulos. 2010. Multiclass defect detection and classification in weld radiographic images using geometric and texture features. Expert Systems with Applications 37, 12 (2010), 7606 – 7614. DOI= http://dx.doi.org/10.1016/j.eswa.2010.04.082

[9] Carrasco M A, Mery D. 2004. Segmentation of welding defects using a robust algorithm. Materials Evaluation,62(11) (2004), 1142-1147.

[10] Y. LeCun, Y. Bengio, and G. Hinton. 2015. Deep learning. Nature, 521(7553) (2015), 436 – 444, DOI= http://dx.doi.org/10.1038/nature14539

[11] Zehuan Yuan, Tong Lu, and Chew Lim Tan. 2017. Learning discriminated and correlated patches for multi-view object detection using sparse coding. Pattern Recognition 69 (2017), 26 – 38. DOI= http://dx.doi.org/10.1016/j.patcog.2017.03.033

[12] Ehsan Hosseini-Asl, Jacek M. Zurada, and Olfa Nasraoui. 2016. Deep Learning of Part-Based Representation of Data Using Sparse Autoencoders With Nonnegativity Constraints. IEEE Transactions on Neural Networks and Learning Systems 27, 12 (2016), 2486 – 2498. DOI= http://dx.doi.org/10.1109/tnnls.2015.2479223

Yan Zhang, Erhu Zhang, and Wanjun Chen. 2016. Deep neural network for halftone image classification based on sparse auto-encoder. Engineering Applications of Artificial Intelligence 50 (2016), 245 – 255. DOI= http://dx.doi.org/10.1016/j.engappai.2016.01.032

[13] D. Mery, V. Riffo, U. Zscherpel, G. Mondrag´on, I. Lillo, I. Zuccar, H. Lobel, and M. Carrasco. 2015. GDXray: The database of X-ray images for nondestructive testing. Journal of Nondestructive Evaluation, 34(4) (2015), 1 – 12. DOI = http://dx.doi.org/10.1007/s10921-015-0315-7.

[14] Nobuyuki Otsu. 1979. A Threshold Selection Method from Gray-Level Histograms. IEEE Transactions on Systems, Man, and Cybernetics 9, 1 (1979), 62 – 66. DOI= http://dx.doi.org/10.1109/tsmc.1979.4310076

Acknowledgments

This work was supported by The National Basic Research Program (973 Program) (Grant nos.2014CB049500), the National Science Foundation of China (Grant nos.51605464) and the Anhui Provincial Natural Science Foundation (Grant nos.1508085QE83).